

Holographic Superconductivity with Gauss-Bonnet gravity

Ruth Gregory

Centre for Particle Theory Durham University, South Road, Durham, DH1 3LE, UK

Abstract. I review recent work ([1, 2]) on holographic superconductivity with Einstein-Gauss-Bonnet gravity, and show how the critical temperature of the superconductor depends on both gravitational backreaction and the Gauss-Bonnet parameter, using both analytic and numerical arguments. I also review computations of the conductivity, finding the energy gap, and demonstrating that there is no universal gap ratio, ω_g/T_c , for these superconductors.

1. Introduction

Holographic superconductivity (see [3, 4, 5] for reviews) is a fascinating idea which proposes to describe strongly coupled high T_c superconductors via a classical gravitational system using the gauge gravity correspondence, [6]. The bulk theory typically has gauge and a charged scalar field, with a black hole providing a finite temperature. Choosing an appropriate scalar potential, such as a negative mass-squared above the Breitenlohner-Friedman bound, [7], allows the scalar to condense out of the vacuum near the black hole horizon, if the curvature is sufficiently large there [8]. This occurs for low temperature black holes, hence the analogy to superconductivity.

The superconducting phase corresponds to a “hairy” black hole, where the condensation of the scalar field out of its symmetric state screens the charge of the black hole. Typical no-hair theorems [9] do not apply in this case as the scalar potential is not positive definite. Near the boundary, the scalar has a power law fall-off, and the coefficient of this fall-off can be interpreted as a condensate in the boundary theory. Following the behaviour of this condensate as the temperature drops reveals the typical behaviour for an order parameter governing the superconducting phase transition, and has been observed in a wide variety of bulk theories, including varying the scalar mass and potential, varying the number of spacetime dimensions, as well as having magnetic fields present and the stability of the system [8, 10, 11, 12, 14, 15, 16]. Similar models have also been found from embeddings in string theory, [17], and it is therefore of interest to consider more general stringy aspects of these models.

In this presentation, I review the results of [1] and [2], which explored adding the higher curvature Gauss-Bonnet (GB) term, [18], to the gravitational action. I will also update on the talk where appropriate, and add a few new results and comments. In brief, many of the qualitative features of the holographic superconductors are stable under higher curvature corrections, however, there are quantitative differences, in particular, a universality relation for an energy gap in the superconductor was found not to be substantiated even in the Einstein limit. (See also [19] for other work on GB holographic superconductors.)

I first review the bulk superconductor, deriving some general analytical results and remarking on the probe superconductor. Then I summarize the numerical results, showing how the

numerical results follow closely an analytical bound, revealing an interesting subtlety in the response of the superconductor to the Gauss-Bonnet parameter α . Finally, I review the results of [1] and [2] on conductivity.

2. The bulk superconductor

The general action is that of an Einstein-Gauss-Bonnet (EGB) gravitational action coupled to a massive charged complex scalar field and a U(1) gauge field:

$$S = \frac{1}{2\kappa^2} \int d^5x \sqrt{-g} \left[-R + \frac{12}{L^2} + \frac{\alpha}{2} \left(R^{abcd} R_{abcd} - 4R^{ab} R_{ab} + R^2 \right) \right] + \int d^5x \sqrt{-g} \left[-\frac{1}{4} F^{ab} F_{ab} + |\nabla_a \psi - iq A_a \psi|^2 - m^2 |\psi|^2 \right] \quad (1)$$

where g is the determinant of the metric, and R_{abcd} , R_{ab} and R are the Riemann curvature tensor, Ricci tensor, and the Ricci scalar, respectively. The Gauss-Bonnet coupling constant is taken in the range $\alpha \in [0, L^2/4]$, and the cosmological constant is given in terms of a length scale, L , which for Einstein gravity ($\alpha = 0$) corresponds to the adS curvature. The Planck scale is set by $\kappa^2 = 8\pi G_5$, q is the charge, and m^2 the (squared) mass, of the scalar field.

The equations of motion satisfied by the bulk system are:

$$R_{ab} - \frac{1}{2} R g_{ab} + \frac{6}{L^2} g_{ab} - \alpha \left[H_{ab} - \frac{1}{4} H g_{ab} \right] = \kappa^2 T_{ab} \quad (2)$$

where

$$H_{ab} = R_a^{cde} R_{bcde} - 2R_{ac} R_b^c - 2R_{acbd} R^{cd} + R R_{ab} , \quad (3)$$

T_{ab} is the matter energy momentum tensor

$$T_{ab} = 2\mathcal{D}_{(a} \psi^\dagger \mathcal{D}_{b)} \psi - F_{ac} F_b^c - \left[|\mathcal{D}_c \psi|^2 - \frac{1}{4} F_{cd}^2 - m^2 |\psi|^2 \right] g_{ab} , \quad (4)$$

and $\mathcal{D}_a = \nabla_a - iq A_a$ is the gauge covariant derivative.

To examine holographic superconductivity, we allow for a bulk black hole in order to have a system at finite temperature:

$$ds^2 = f(r) e^{2\nu(r)} dt^2 - \frac{dr^2}{f(r)} - \frac{r^2}{L_e^2} (dx^2 + dy^2 + dz^2) \quad (5)$$

where

$$f(r) = \frac{r^2}{2\alpha} \left[1 - \sqrt{1 - \frac{4\alpha}{L^2} \left(1 - \frac{r_+^4}{r^4} \right)} \right] \quad (6)$$

is the black hole gravitational potential in the absence of backreaction, and

$$L_e^2 = \frac{L^2}{2} \left[1 + \sqrt{1 - \frac{4\alpha}{L^2}} \right] \quad (7)$$

is the actual curvature of the adS spacetime, which is renormalized away from the cosmological constant scale, L , once α is nonzero. The temperature of the background is:

$$T = \frac{1}{4\pi} f'(r_+) e^{\nu(r_+)} , \quad (8)$$

which is equal to $r_+/\pi L^2$ in the absence of backreaction.

Taking a static ansatz, $A_\mu = (\phi(r), 0, \dots)$ and $\psi = \psi(r)$ (which can be taken to be real), the equations of motion become

$$\phi'' + \left(\frac{3}{r} - \nu'\right) \phi' - 2q^2 \frac{\psi^2}{f} \phi = 0, \quad (9)$$

$$\psi'' + \left(\frac{3}{r} + \nu' + \frac{f'}{f}\right) \psi' + \left(\frac{q^2 \phi^2}{f^2 e^{2\nu}} - \frac{m^2}{f}\right) \psi = 0, \quad (10)$$

$$\left(1 - \frac{2\alpha f}{r^2}\right) \nu' = \frac{2\kappa^2}{3} r \left(\psi'^2 + \frac{q^2 \phi^2 \psi^2}{f^2 e^{2\nu}}\right) \quad (11)$$

$$\left(1 - \frac{2\alpha f}{r^2}\right) f' + \frac{2}{r} f - \frac{4r}{L^2} = -\frac{2\kappa^2}{3} r \left[\frac{\phi'^2}{2e^{2\nu}} + m^2 \psi^2 + f \psi'^2 + \frac{q^2 \phi^2 \psi^2}{f e^{2\nu}}\right] \quad (12)$$

where a prime denotes derivative with respect to r . These equations have several scaling symmetries, as noted in [2], which are used to set $L = Q = q = 1$. Note that by fixing $Q = 1$, the charge parameter is kept fixed in all numerical computations.

- (i) $r \rightarrow ar, t, x^i \rightarrow at, ax^i, L \rightarrow aL, q \rightarrow q/a, \alpha \rightarrow a^2 \alpha, A \rightarrow aA$.
- (ii) $r \rightarrow br, t \rightarrow t/b, x^i \rightarrow x^i/b, f \rightarrow b^2 f, \phi \rightarrow b\phi$.
- (iii) $\phi \rightarrow c\phi, \psi \rightarrow c\psi, q \rightarrow q/c, \kappa^2 \rightarrow \kappa^2/c^2$.

The horizon is defined in general by $f(r_+) = 0$, and demanding regularity of the solution at both the horizon and boundary gives the following boundary conditions:

- Horizon:

$$\phi(r_+) = 0, \quad \psi'(r_+) = \frac{m^2}{f'(r_+)} \psi(r_+) \quad (13)$$

$$\nu'(r_+) = \frac{2\kappa^2}{3} r_+ \left(\psi'(r_+)^2 + \frac{\phi'(r_+)^2 \psi(r_+)^2}{f'(r_+)^2 e^{2\nu(r_+)}}\right) \quad (14)$$

$$f'(r_+) = \frac{4}{L^2} r_+ - \frac{2\kappa^2}{3} r_+ \left(\frac{\phi'(r_+)^2}{2e^{2\nu(r_+)}} + m^2 \psi(r_+)^2\right) \quad (15)$$

- Boundary:

$$\nu \rightarrow 0, \quad f(r) \sim \frac{r^2}{L_e^2} \Rightarrow \quad (16)$$

$$\phi(r) \sim P - \frac{Q}{r^2}, \quad \psi(r) \sim \frac{C_-}{r^{\Delta_-}} + \frac{C_+}{r^{\Delta_+}}, \quad \text{as } r \rightarrow \infty, \quad (17)$$

where $\Delta_\pm = 2 \pm \sqrt{4 + m^2 L_e^2}$ for a general mass m^2 . We choose $C_- = 0$, then P and C_+ are fixed by consistency with the near horizon solution. According to the AdS/CFT correspondence, we can interpret $\langle \mathcal{O}_{\Delta_+} \rangle \equiv C_+$, where \mathcal{O}_{Δ_+} is the operator with the conformal dimension Δ_+ dual to the scalar field.

In [1] we chose to set the mass of the scalar field as $m^2 = -3/L^2$, so that the mass remained the same as α was varied. However, the variation of the effective asymptotic AdS curvature, (7), with α relative to L means that this mass actually *increases* (i.e. becomes less negative) with respect to the asymptotic AdS scale, and therefore the dimension of the boundary operator corresponding to C_+ varies with α . Fixing $m^2 = -3/L_{\text{eff}}^2$ relative to the asymptotic AdS scale, avoids this problem, however the mass now varies with respect to the physical mass and temperature of the black hole as α varies. See [20] for a detailed examination of the effect of scalar mass on the holographic superconductor.

2.1. Analytic bounds

While the equations of motion (9-12) require a numerical solution in general, even in the absence of backreaction, near the critical temperature we can glean a measure of analytic information using the (uncondensed) charged black hole solution, [21]:

$$A = \phi_0(r)dt = \frac{Q}{r_+^2} \left(1 - \frac{r_+^2}{r^2}\right) dt \quad (18)$$

$$\nu_0 = 0 \quad (19)$$

$$f_0(r) = \frac{r^2}{2\alpha} \left[1 - \sqrt{1 - \frac{4\alpha}{L^2} \left(1 - \frac{r_+^4}{r^4}\right) + \frac{8\alpha\kappa^2 Q^2}{3r^4 r_+^2} \left(1 - \frac{r_+^2}{r^2}\right)} \right] \quad (20)$$

and linearizing in the scalar condensate. In the above, Q is the charge of the black hole (up to a geometrical factor of 4π), and r_+ is the event horizon, which determines the “ADM” mass of the black hole [22]. To avoid a naked singularity, we restrict the parameter range as $\alpha \leq L^2/4$.

Linearizing in the scalar condensate leaves the background solution for the metric and gauge field unchanged to leading order, and we can focus on (10) with f and ϕ taking their background values. Analytic bounds on the critical temperature can be obtained by looking for simple relations that must hold for the existence of a nontrivial scalar solution. First consider the variable $X_n = r^n \psi$, which satisfies to leading order:

$$X_n'' + \left(\frac{f_0'}{f_0} - \frac{3-2n}{r} \right) X_n' + \left(\frac{q^2 \phi^2}{f_0^2} - \frac{m^2}{f_0} - \frac{n f_0'}{r f_0} + \frac{n(n-2)}{r^2} \right) X_n = 0. \quad (21)$$

To get an upper bound, let $n = 2$, and consider the general properties of a solution. At the horizon,

$$X_2'(r_+) = \frac{X_2(r_+)}{4\pi T_c} \left(\frac{8}{L^2} + m^2 - \frac{8\kappa^2 Q^2}{3r_+^6} \right) \quad (22)$$

which is positive for small $\kappa^2 Q^2$ (taking $X_2(r_+) > 0$ without loss of generality). Since $X_2 \sim 1/r^{2+\Delta_+}$ as $r \rightarrow \infty$, the solution must have a maximum for some r , which requires that

$$\left(\frac{q^2 \phi^2}{f_0^2} - \frac{m^2}{f_0} - \frac{2f_0'}{r f_0} \right) > 0 \quad (23)$$

at this point. An examination of when this combination is never positive provides an upper bound for T_c . (A different n was used in [1], which sufficed for the probe limit although it led to a looser bound. For consistency and comparison between the scalar masses, this new bound is used here.)

We can also obtain a lower bound by considering $n = 3$. Manipulating (21) shows that if a solution exists, then the integral

$$\int_{r_+}^{\infty} \frac{1}{r^3} \left[\frac{\phi_0^2}{f_0} - m^2 + \frac{3f_0}{r^2} - \frac{3f_0'}{r} \right] = - \int_{r_+}^{\infty} \frac{f_0 X_3'^2}{r^3 X_3^2} \leq 0 \quad (24)$$

is negative. Note that negativity of this integral does not imply existence of a solution to the linearized equation near T_c , it is simply a necessary condition. Since this integral is always negative at large T , and positive as $T \rightarrow 0$ (for $\kappa^2 \lesssim 0.4$), observing where it changes sign provides a lower bound on T_c . This bound was found to give an extremely reliable indicator of T_c as computed numerically.

2.2. Analytic expansion

In instances where the exact solution is only known numerically, it can be useful to derive an analytic approximation to the exact solution using a technique of matching. The solution is Taylor expanded around the horizon and boundary, then matched at a midpoint. This technique was used in [1] to get an approximation to T_c , although the plot in [1] was inaccurate. In brief, we first transform the radial variable to $z = r_+/r$, and expand the near horizon solution of a generic field Y as:

$$Y \simeq Y_0 - Y_1(1 - z) + \frac{1}{2}Y_2(1 - z)^2 \quad (25)$$

The equations of motion give:

$$\psi_1 = \frac{m^2 r_+^2}{f_1} \psi_0 \quad (26)$$

$$\psi_2 = \frac{\psi_0}{2f_1^2} \{m^2 r_+^2 f_2 - m^2 r_+^2 f_1 \nu_1 + m^4 r_+^4 - q^2 \phi_1^2 r_+^2 e^{-2\nu_0} - 3m^2 r_+^2 f_1\} \quad (27)$$

$$\phi_2 = \phi_1 \left(1 + \nu_1 + \frac{2r_+^2 q^2 \psi_0^2}{f_1} \right) \quad (28)$$

where f_1 , f_2 , and ν_1 are given by (11,12), and depend on ϕ_0 and ψ_0 . Since the asymptotic solutions for the gauge and scalar field given by (17) also have two unknowns, matching these fields and their derivatives at some intermediate point z_0 gives four equations which determine these four unknowns:

$$P - \frac{Qz_0^2}{r_+^2} = -\phi_1(1 - z_0) + \frac{\phi_2}{2}(1 - z_0)^2 \quad (29)$$

$$\frac{-2Qz_0}{r_+^2} = \phi_1 - \phi_2(1 - z_0) \quad (30)$$

$$\frac{C_+ z_0^{\Delta_+}}{r_+^{\Delta_+}} = \psi_0 - \psi_1(1 - z_0) + \frac{\psi_2}{2}(1 - z_0)^2 \quad (31)$$

$$\Delta_+ \frac{C_+ z_0^{\Delta_+ - 1}}{r_+^{\Delta_+}} = \psi_1 - \psi_2(1 - z_0) \quad (32)$$

Clearly, given the complexity of the expressions (26)-(28), which themselves contain f_i , this is a rather involved algebraic process in the general backreacting and non-critical case. Nonetheless, the system is tractable analytically if we simply focus on deriving the critical temperature. In this case, we once again can take the background forms for ϕ , f and ν , which considerably reduce the complexity of the relations: (29) and (30) are automatically satisfied, $\nu \equiv 0$, (12) gives

$$f_1 = -4\frac{r_+^2}{L^2} + \frac{\kappa^2 \phi_1^2}{3} \quad (33)$$

$$f_2 = -f_1 + \frac{2\alpha f_1^2}{r_+^2} + 2\kappa^2 \phi_1^2 \quad (34)$$

and consistency of the ψ equations (31) and (32) implies

$$2\Delta_+ \psi_0 - 2(\Delta_+ + (1 - \Delta_+)z_0) \psi_1 + (\Delta_+ - 2(\Delta_+ - 1)z_0 + (\Delta_+ - 2)z_0^2) \psi_2 = 0 \quad (35)$$

Although this is a cumbersome expression for nonzero κ^2 , it is just a quadratic for $\phi_1^2/r_+^2 = 4Q^2/r_+^6$, and a linear relation in the probe limit, which in either case can be straightforwardly

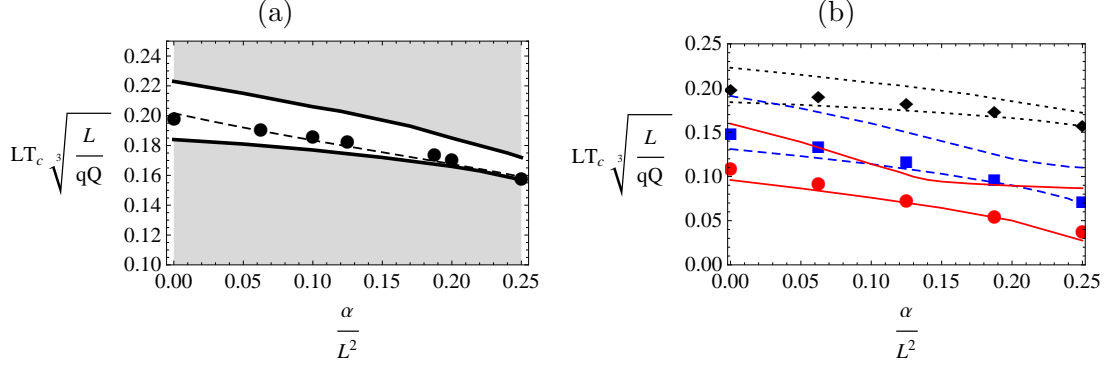


Figure 1. A plot of the critical temperature as a function of α for the scalar mass $m^2 = -3/L^2$. (a) shows a detailed plot of the probe limit, with upper and lower bounds shown as solid black lines, the matching method value as a dotted line, and numerical data points. (b) shows a plot of the upper and lower bounds together with exact numerical results for the probe limit in black (dotted lines and diamond data points), $\kappa^2 = 0.05$ in blue (dashed lines and square data points), and $\kappa^2 = 0.1$ in red (solid lines and circular data points).

solved and the critical temperature obtained from

$$T_c = r_+ \left[\frac{1}{\pi L^2} - \frac{\kappa^2 Q^2}{3r_+^6} \right] \quad (36)$$

It only remains to choose a value for z_0 . In [1] the value $z_0 = 1/2$ was chosen to be specific, however, this choice does not take into account the variation of the effective adS length scale with α . In essence, the matching point should be chosen to represent where the asymptotic expansion $f \simeq r_+^2/z^2 L_e^2$ turns over into the near horizon expansion. This obviously depends on the relative ratio of r_+ to L_e , although as $\alpha \rightarrow L^2/4$ this point moves rather significantly towards the boundary. A good approximation to the departure from the asymptotic regime is $z_0 \simeq \alpha/L^2 + 1/2$, which is the value used in figure 1(a). It must be noted however, that there is a degree of arbitrariness in this matching process. Although the choice of z_0 attempts to take into account the likely variation of the domains of validity of each expansion with α , this is a rather ad hoc process, and as backreaction is switched on, the matching procedure becomes less and less reliable. It is included here for completeness, however by far the best analytic guide to critical temperature is the lower bound.

2.3. Discussion of analytic results

By examining the behaviour of a putative condensed scalar in the bulk, it is possible to derive upper and lower bounds to the critical temperature. A matching method can also be used to get an approximate solution for the scalar, however, this method (as well as the upper bound) becomes unreliable as the backreaction is increased. On the other hand, the lower bound appears to be extremely representative of the behaviour of the actual critical temperature, and works well for a significant range of backreaction. Figures 1 and 2 show the analytical results, and will be discussed further together with numerical data in the next section.

3. Backreacting superconductors

In order to find the actual behaviour of the bulk superconductor, in [1] and [2] we integrated (9–12) numerically. As already stated, we took $L = Q = q = 1$, and varied r_+ to study how

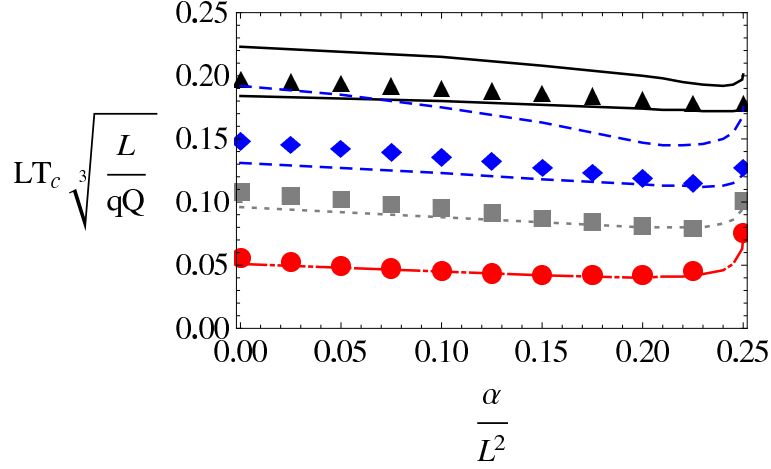


Figure 2. A plot of the critical temperature as a function of α for a selection of κ^2 . The analytic bounds are shown as lines and the numerical data as points. Respectively: $\kappa^2 = 0$ is shown in black, with solid lines and triangular data points; $\kappa^2 = 0.05$ has blue dashed lines and diamonds; $\kappa^2 = 0.1$ has a grey dotted line and squares; $\kappa^2 = 0.2$ has a red dot-dash line with circular data points. The lower bound is shown for all κ^2 values, but the upper bound is shown only for the lowest two values of κ^2 , as they overlap significantly with the other data and confuse the plot.

the system reacted to varying temperature. From these numerical solutions, we can deduce the critical temperature, determine the behaviour of the condensate with temperature, and compute the conductivity of the holographic superconductor as discussed in subsection 3.3.

3.1. The dependence of T_c on α and κ^2 .

The analytic bounds for T_c have been plotted in figures 1 and 2 together with the exact values of T_c obtained by numerical computation for both masses of the scalar field. For $m^2 = -3/L_e^2$, both bounds are shown, as well as the matching method result for the probe limit. For $m^2 = -3/L_e^2$, the upper bound has only been shown for $\kappa^2 \leq 0.05$, as above this value it becomes less predictive and clutters the plot, and indeed beyond $\kappa^2 \sim 0.2$ (corresponding to $q \sim 2.25$ in the notation of [10]) it ceases to have quantitative value for any α . The lower bound on the other hand becomes successively more accurate as the values of κ^2 are stepped up, and gives a very good quantitative guide to the behaviour of T_c as we vary α and κ^2 .

It is easy to see that in all cases, the effect of backreaction is to decrease T_c and thus make condensation harder. We can see this by using Gubser's rough argument, [8], that the effective scalar mass $m_{\text{eff}}^2 = m^2 - q^2\phi(r)^2/f(r)$ becomes more negative as backreaction is turned up. Essentially, the effect of backreaction is that the condensation of the scalar field not only screens the charge of the black hole, but also its mass, as the scalar and gauge fields now contribute to the ADM mass. This means that for a given charge and temperature, the radius of the black hole is increased, which makes it harder for the scalar to condense.

One very interesting feature clearly exhibited in the bounds is the turning point in T_c as a function of α for the mass $m^2 = -3/L_e^2$. In the probe case, this occurs very near the Chern-Simons limit $\alpha = L^2/4$, and is barely perceptible in the numerical data, however once backreaction is switched on, the minimum becomes much more pronounced, and indeed for large backreaction ($\kappa^2 = 0.2$) the Chern-Simons limit is showing a considerable enhancement of T_c over the typical values for lower α .

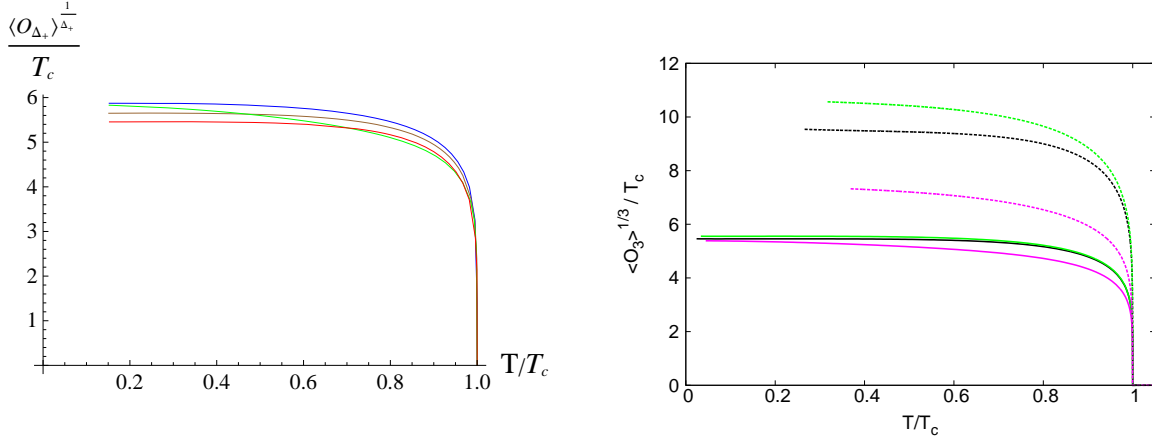


Figure 3. Two plots of the condensate as a function of temperature for $m^2 = -3/L^2$ (left) and $m^2 = -3/L_e^2$ (right). The plot on the left shows several values of α in the probe limit: $\alpha = 0$ in red, the lowest line, then $\alpha = 0.1$ in brown, 0.2 in blue and 0.25 in green. The plot on the right shows $\kappa^2 = 0$ in solid lines, and $\kappa^2 = 0.1$ as dotted lines. The black plot is $\alpha = 0$, green is $\alpha = 0.125$ and magenta is $\alpha = 0.25$.

3.2. The scalar condensate.

The numerical results allow a full exploration of the dependence of the condensate on temperature, and we expect to see the condensate switching on sharply at the critical temperature, then saturating at low temperatures, and this is indeed what is seen. Figure 3 shows $\langle \mathcal{O}_{\Delta_+} \rangle^{1/\Delta_+}$ as a function of temperature for both scalar masses.

Each line in the plot shows the characteristic curve of the condensate $\langle \mathcal{O}_{\Delta_+} \rangle^{1/\Delta_+}$ condensing at some critical temperature. For $m^2 = -3/L^2$ the curves are shown in the probe limit. While the critical temperature does not display the minimum in α , it can nonetheless be seen that the Chern-Simons limit does look rather different, and the scalar field saturates far more slowly as the temperature drops. For $m^2 = -3/L_e^2$, three different values of α (0, 0.125, 0.25) and two different values of κ^2 (0, 0.1) are chosen to display the features of the system. Both plots are shown with the curves normalized by T_c . In the latter plot, the effect of κ^2 is to increase the height of these graphs, in spite of the fact that the raw data tends to have lower values of $\langle \mathcal{O}_3 \rangle$. This is clearly because the most significant impact of increasing gravitational backreaction is that the critical temperature of the system is lowered. In this case the effect of backreaction is extremely marked, with the condensate varying more widely with α .

3.3. Conductivity

In [11], Horowitz and Roberts observed an interesting phenomenon for the conductivity of the boundary theory. They considered the model (1) in the probe Einstein limit for a range of different bulk scalar masses, and on computing the conductivity found an apparent universal relation

$$\frac{\omega_g}{T_c} \simeq 8, \quad (37)$$

with deviations of less than 8 %.

Conductivity is conventionally expressed as the current density response to an applied electric field:

$$\sigma = \frac{\mathcal{J}}{\mathcal{E}}. \quad (38)$$

The boundary four-current J_μ is dual to the bulk field A_μ , thus we must consider perturbations of A_μ to compute the conductivity. The full perturbation problem must take into account perturbations of the metric (h_{ti} and h_{ri}) and the perturbation of the Gauss-Bonnet tensor H_{ti}, H_{ri} . After some algebra, these reduce to:

$$\dot{h}'_{ti} - \frac{2}{r}\dot{h}_{ti} - \ddot{h}_{ri} + \frac{L^2 f e^{2\nu}}{r^2 - 2\alpha f} \left(1 - \frac{\alpha(2\nu' f + f')}{r}\right) \Delta h_{ri} + \frac{2\kappa^2 r^2 \dot{A}_i \phi'}{r^2 - 2\alpha f} = 0 \quad (39)$$

$$\frac{e^{-\nu}}{r f} [r f e^\nu A'_i]' - \frac{\ddot{A}_i}{f^2 e^{2\nu}} + \frac{L^2}{r^2 f} \Delta A_i - \frac{2}{f} q^2 \psi^2 A_i + \frac{\phi'}{f e^{2\nu}} \left(h'_{ti} - \frac{2}{r} h_{ti} - \dot{h}_{ri}\right) = 0 \quad (40)$$

where h_{ab} is the perturbation of the metric tensor, and A_i is the perturbation of the gauge field, which has only spatial components. Writing $A_i(t, r, x^i) = A(r) e^{i\mathbf{k}\cdot\mathbf{x} - i\omega t} e_i$, and setting $\mathbf{k} = \mathbf{0}$, (39) can be integrated and substituted in (40) to obtain:

$$A'' + \left(\frac{f'}{f} + \nu' + \frac{1}{r}\right) A' + \left[\frac{\omega^2}{f^2 e^{2\nu}} - \frac{2}{f} q^2 \psi^2 - \frac{2\kappa^2 r^2 \phi'^2}{f e^{2\nu} (r^2 - 2\alpha f)}\right] A = 0. \quad (41)$$

This is solved under the physically imposed boundary condition of no outgoing radiation at the horizon:

$$A(r) \sim f(r)^{-i\frac{\omega}{4\pi T_+}}, \quad (42)$$

where T_+ is the temperature. In the asymptotic adS region ($r \rightarrow \infty$), the general solution takes the form

$$A = a_0 + \frac{a_2}{r^2} + \frac{a_0 L_e^4 \omega^2}{2r^2} \log \frac{r}{L} \quad (43)$$

where a_0 and a_2 are integration constants. Note there is an arbitrariness of scale in the logarithmic term, as pointed out in [11], however, this is related to an arbitrariness in the holographic renormalization process; see Appendix A of [2] for a full computation of the conductivity and discussion of this renormalization scale. After careful computation using the method of Skenderis [23], the conductivity of the EGB system is found to be [2]:

$$\sigma = \frac{2a_2}{i\omega L_e^4 a_0} + \frac{i\omega}{2} - i\omega \log \left(\frac{L_e}{L}\right). \quad (44)$$

Note that the imaginary term linear in ω has an arbitrariness of scale from the counterterm subtraction, and this is capitalized in the presentation of numerical data, where a suitable renormalization scale is chosen to make the features of the plot clearest.

Figure 4 shows the real and imaginary parts of the conductivity as a function of ω/T_c , calculated for the scalar mass $m^2 = -3/L^2$ in the probe limit and for a selection of values of α/L^2 . These plots clearly show that as α increases, the normalised gap frequency shifts to higher values. An additional feature is that the gap becomes softer with increasing α . These plots should be contrasted with figure 5, which shows similar conductivity plots, but now for scalar mass $m^2 = -3/L_e^2$, and with both no backreaction and a backreaction of $\kappa^2 = 0.05$. Three sample values of α are shown: 0, 0.125, and 0.25. In these plots, the gap if anything gets harder with increasing α , however once backreaction is included, the gap becomes more gentle and extended, and while the dip in $\text{Im}(\sigma)$ is smoothed, it is still clearly apparent.

In all of these plots, the gap is clearly indicated by a rise in the real part of σ , which coincides with the global minimum of $\text{Im}(\sigma)$. As already noted, the imaginary part of (44) is only valid up to a linear term in ω , the size of which is dependent on the renormalization scheme employed (and also on the charge Q). One can therefore tune this linear term in $\text{Im}(\sigma)$ to create a finite global minimum if it is not initially present, and indeed the plots in figure 4 differ from those

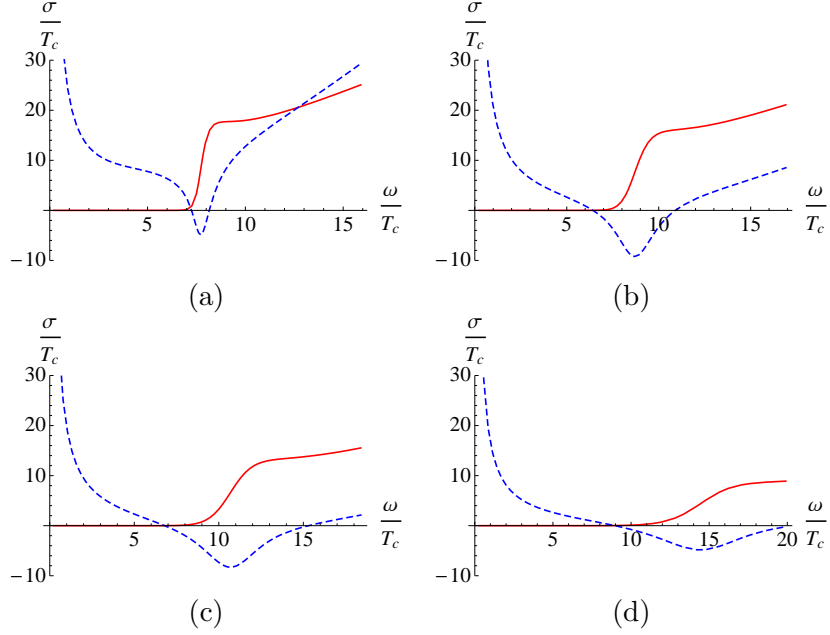


Figure 4. Conductivity: a range of plots showing the real (solid red line) and imaginary (blue dashed line) parts of the (normalized) conductivity as a function of (normalized) frequency for the scalar mass $m^2 = -3/L^2$. Plot (a) is $\alpha = 0$, (b) is $\alpha = 0.1$, and (c) is $\alpha = 0.2$, and (d) is $\alpha = 0.25$.

presented in [1] by precisely this sort of term so as to make the minimum apparent. This minimum can therefore be used to define ω_g , the value of the frequency gap.

The frequency gap is a distinct characteristic of a superconductor and in the BCS theory of superconductivity this frequency gap corresponds to the minimum energy required to break a Cooper pair. As mentioned above, in [11] it was claimed that for the holographic superconductor the relation $\omega_g/T_c \simeq 8$ had a certain universality, proving stable for a range of scalar masses and dimensions. In both [1] and [2], this relation was shown to be unstable to Gauss-Bonnet corrections. Figure 5(d) in particular gives a very clear indicator of how backreaction and higher curvature terms affect the gap. Increasing either α or κ^2 increases ω_g/T_c . For the case of increasing α , the effect occurs mainly because of a shift in the gap, rather than a significant alteration of T_c , which varies much more strongly with backreaction than α . On the other hand, varying κ^2 practically does not alter ω_g at all, whereas T_c drops dramatically, leading to a sharp rise in ω_g/T_c .

4. Summary

This presentation reviewed the work of [1] and [2] on exploring the implications of Gauss-Bonnet corrections to holographic superconductors. The results show that increasing backreaction lowers the critical temperature of the superconductor hence increasing ω_g/T_c . The effect of higher curvature terms is more subtle. Although these initially act in a similar fashion to backreaction in lowering the critical temperature, for significant GB coupling and larger scalar masses, the critical temperature eventually begins to increase. The conductivity gap is also modified, with both ω_g and T_c altering to increase the ratio ω_g/T_c . Clearly higher dimensional holographic superconductors have a rich structure, with or without higher curvature corrections.

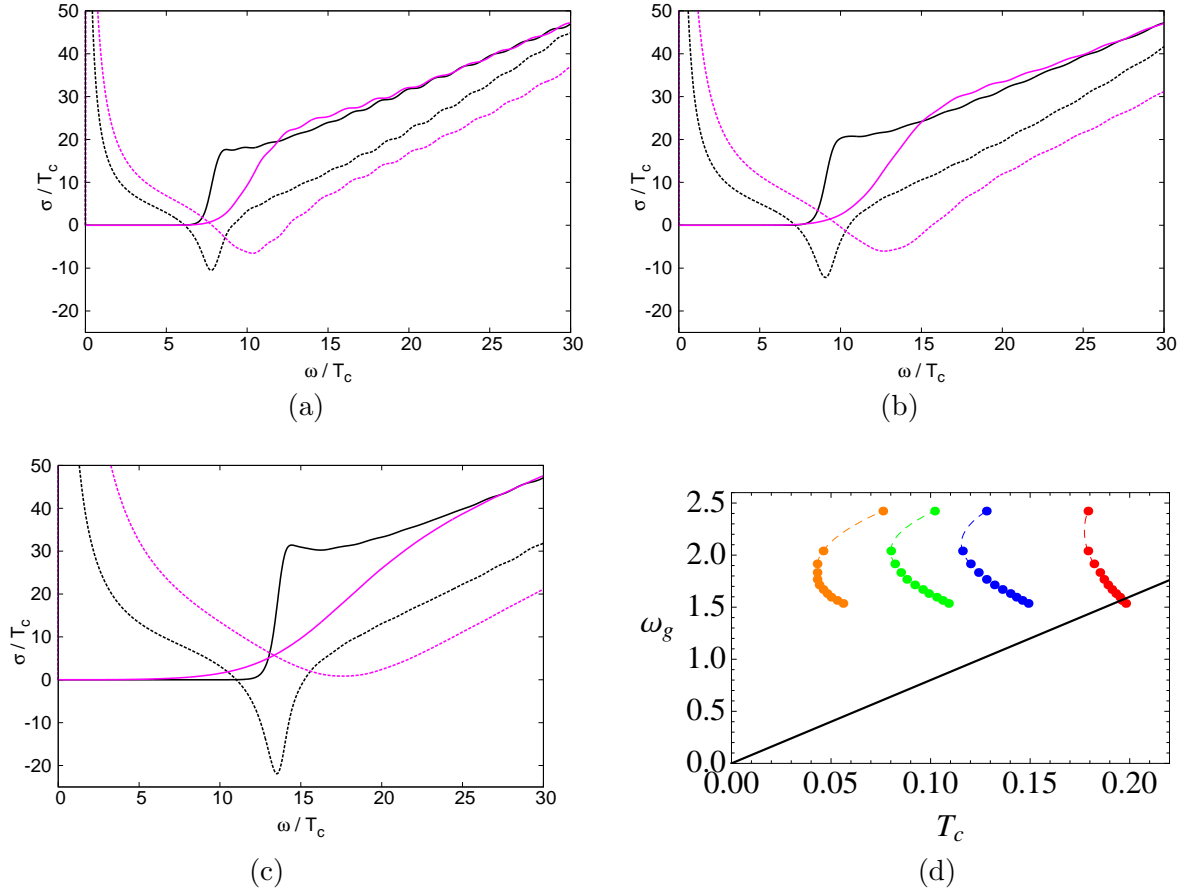


Figure 5. Conductivity: a range of plots showing the conductivity of the $m^2 = -3/L_e^2$ superconductor. Plots (a) – (c) show the real (solid line) and imaginary (dashed line) parts of the conductivity as a function of frequency for $\alpha = 0, 0.125$, and 0.25 respectively. In each case the conductivity is shown for no backreaction in black, and for a backreacting parameter $\kappa^2 = 0.05$ in magenta. The slight undulations in the plots at large ω is a numerical artefact. Plot (d) shows the gap frequency as a function of T_c with the line $\omega_g = 8T_c$ is shown in black. The different colours represent from right to left: Red is $\kappa^2 = 0$, Blue is $\kappa^2 = 0.05$, Green 0.1 , and Orange $\kappa^2 = 0.2$. In each case α is incremented from 0 to 0.25 . As the gap alters rapidly near the Chern-Simons limit, the dotted lines are added by hand to guide the eye.

Acknowledgments

I would like to thank Luke Barclay, Sugumi Kanno, Jiro Soda and Paul Sutcliffe for being such lively and pleasant collaborators. I would also like to thank Christos Charmousis, Rob Myers and Simon Ross for useful conversations. I acknowledge the support of STFC under the rolling grant ST/G000433/1.

References

- [1] R. Gregory, S. Kanno and J. Soda, JHEP **0910**, 010 (2009) [arXiv:0907.3203 [hep-th]].
- [2] L. Barclay, R. Gregory, S. Kanno and P. Sutcliffe, “Gauss-Bonnet Holographic Superconductors,” arXiv:1009.1991 [hep-th].
- [3] C. P. Herzog, J. Phys. A **42**, 343001 (2009) [arXiv:0904.1975 [hep-th]].
- [4] S. A. Hartnoll, Class. Quant. Grav. **26**, 224002 (2009) [arXiv:0903.3246 [hep-th]].

- [5] G. T. Horowitz, “Introduction to Holographic Superconductors,” arXiv:1002.1722 [hep-th].
- [6] J. M. Maldacena, Adv. Theor. Math. Phys. **2**, 231 (1998) [Int. J. Theor. Phys. **38**, 1113 (1999)] [arXiv:hep-th/9711200].
- [7] P. Breitenlohner and D. Z. Freedman, Annals Phys. **144**, 249 (1982).
- [8] S. S. Gubser, Class. Quant. Grav. **22**, 5121 (2005) [arXiv:hep-th/0505189].
Phys. Rev. D **78**, 065034 (2008) [arXiv:0801.2977 [hep-th]].
- [9] J. D. Bekenstein, “Black hole hair: Twenty-five years after,” arXiv:gr-qc/9605059.
T. Hertog, Phys. Rev. D **74**, 084008 (2006) [arXiv:gr-qc/0608075].
- [10] S. A. Hartnoll, C. P. Herzog and G. T. Horowitz, Phys. Rev. Lett. **101**, 031601 (2008) [arXiv:0803.3295 [hep-th]].
S. A. Hartnoll, C. P. Herzog and G. T. Horowitz, JHEP **0812**, 015 (2008) [arXiv:0810.1563 [hep-th]].
- [11] G. T. Horowitz and M. M. Roberts, Phys. Rev. D **78**, 126008 (2008) [arXiv:0810.1077 [hep-th]].
- [12] S. S. Gubser and A. Nellore, Phys. Rev. D **80**, 105007 (2009) [arXiv:0908.1972 [hep-th]].
G. T. Horowitz and M. M. Roberts, JHEP **0911**, 015 (2009) [arXiv:0908.3677 [hep-th]].
R. A. Konoplya and A. Zhidenko, Phys. Lett. B **686**, 199 (2010) [arXiv:0909.2138 [hep-th]].
- [13] S. S. Gubser and S. S. Pufu, JHEP **0811**, 033 (2008) [arXiv:0805.2960 [hep-th]].
K. Peeters, J. Powell and M. Zamaklar, JHEP **0909**, 101 (2009) [arXiv:0907.1508 [hep-th]].
- [14] K. Maeda, M. Natsuume and T. Okamura, Phys. Rev. D **79**, 126004 (2009) [arXiv:0904.1914 [hep-th]].
- [15] E. Nakano and W. Y. Wen, Phys. Rev. D **78**, 046004 (2008) [arXiv:0804.3180 [hep-th]].
T. Albash and C. V. Johnson, JHEP **0809**, 121 (2008) [arXiv:0804.3466 [hep-th]].
- [16] T. Takahashi and J. Soda, Phys. Rev. D **79**, 104025 (2009) [arXiv:0902.2921 [gr-qc]].
S. Kanno and J. Soda, Phys. Rev. D **82**, 086003 (2010) [arXiv:1007.5002 [hep-th]].
- [17] S. S. Gubser, C. P. Herzog, S. S. Pufu and T. Tesileanu, Phys. Rev. Lett. **103**, 141601 (2009) [arXiv:0907.3510 [hep-th]].
J. P. Gauntlett, J. Sonner and T. Wiseman, Phys. Rev. Lett. **103**, 151601 (2009) [arXiv:0907.3796 [hep-th]].
- [18] D. Lovelock, J. Math. Phys. **12**, 498 (1971).
- [19] Q. Pan, B. Wang, E. Papantonopoulos, J. Oliveira and A. B. Pavan, Phys. Rev. D **81**, 106007 (2010) [arXiv:0912.2475 [hep-th]].
X. H. Ge, B. Wang, S. F. Wu and G. H. Yang, JHEP **1008**, 108 (2010) [arXiv:1002.4901 [hep-th]].
Y. Brihaye and B. Hartmann, Phys. Rev. D **81**, 126008 (2010) [arXiv:1003.5130 [hep-th]].
Q. Pan and B. Wang, Phys. Lett. B **693**, 159 (2010) [arXiv:1005.4743 [hep-th]].
R. G. Cai, Z. Y. Nie and H. Q. Zhang, Phys. Rev. D **82**, 066007 (2010) [arXiv:1007.3321 [hep-th]].
M. Siani, “Holographic Superconductors and Higher Curvature Corrections,” arXiv:1010.0700 [hep-th].
- [20] Luke Barclay, in preparation.
- [21] D. G. Boulware and S. Deser, Phys. Rev. Lett. **55**, 2656 (1985).
R. G. Cai, Phys. Rev. D **65**, 084014 (2002) [arXiv:hep-th/0109133].
- [22] L. F. Abbott and S. Deser, Nucl. Phys. B **195**, 76 (1982).
S. Deser and B. Tekin, Phys. Rev. D **67**, 084009 (2003) [arXiv:hep-th/0212292].
- [23] K. Skenderis, Class. Quant. Grav. **19**, 5849 (2002) [arXiv:hep-th/0209067].